

Exploring the dynamics and interaction of a full ErbB2 receptor and Trastuzumab-Fab antibody in a lipid bilayer model using Martini coarse-grained force field

Juan Felipe Franco-Gonzalez · Javier Ramos ·
Victor L. Cruz · Javier Martinez-Salazar

Received: 31 January 2014/Accepted: 7 August 2014/Published online: 17 August 2014
© Springer International Publishing Switzerland 2014

Abstract Coarse grained (CG) modeling has been applied to study the influence of the Trastuzumab monoclonal antibody on the structure and dynamics of the full ErbB2 receptor dimer, including the lipid bilayer. The usage of CG models to study such complexes is almost mandatory, at present, due to the large size of the whole system. We will show that the Martini model performs satisfactorily well, giving results well-matched with those obtained by atomistic models as well as with the experimental information existing on homolog receptors. For example, the extra and intracellular domains approach the bilayer surface in both the monomer and dimer cases. The Trastuzumab-Fab hinders the interaction of the receptors with the lipid bilayer. Another interesting effect of the antibody is the disruption of the antiparallel arrangement of the juxtamembrane segments in the dimer case. These findings might help to understand the effect of the antibody on the receptor bioactivity.

Keywords Coarse grained · Molecular dynamics simulation · Martini · ErbB2 · Trastuzumab

Introduction

The epidermal growth factor receptors (EGFRs) are a family of membrane proteins associated to a number of biological processes involving, among others, cellular proliferation. The over expression of some of these receptors at the cell surface has been associated with aggressive forms of cancer and low survival rate [1]. In particular, ErbB2 over expression on breast cancer cells was identified as a negative factor affecting cancer progression and final survival time [2, 3]. Thus, the monoclonal antibody Trastuzumab was designed to target an extracellular epitope of the ErbB2 receptor [4–6], being the first specific anti-ErbB2 treatment approved by the Food and Drug Administration (FDA). However, the molecular mechanism of action of Trastuzumab is not at all understood. Different effects have been reported regarding its anticancer activity [7–9]. For example, Trastuzumab has been identified as an inhibitor of the downstream signaling cascade for cellular proliferation by its action through a number of different mechanisms.

Structurally, the ErbB2 receptor consists of three domains, namely, the extracellular domain (ECD), a transmembrane domain consisting of one alpha-helix and a cytoplasmic domain containing the active site tyrosine-kinase (TKD) necessary for signaling. The ErbB2 epitope targeted by Trastuzumab is located in subdomain IV of the ECD. The tight interaction of the monoclonal antibody Fab with subdomain IV of the ErbB2 was elucidated by crystallography [10]. Additionally, molecular dynamics simulations performed at the atomistic scale on the complex have shown an additional interaction between the antibody constant domain and the dimerization arm located in sub-domain II of the receptor [11, 12]. The authors argued that the additional interaction does not appear in the

Electronic supplementary material The online version of this article (doi:[10.1007/s10822-014-9787-2](https://doi.org/10.1007/s10822-014-9787-2)) contains supplementary material, which is available to authorized users.

J. F. Franco-Gonzalez · J. Ramos · V. L. Cruz (✉) ·
J. Martinez-Salazar
Biophysm, Macromolecular Physics Department, Instituto de
Estructura de la Materia, CSIC, Serrano 113-bis, 28006 Madrid,
Spain
e-mail: victor.cruz@iem.cfmac.csic.es

crystallographic structures due to strong crystal packing conditions which are not present in solution.

So far, most of the structural studies, either computational or experimental, performed on the EGFR family members have been carried out separately on ECD [10, 13–17], transmembrane [18–28] and TKD [29–40]. The inherent difficulties associated to both the presence of the membrane and the size of the full systems are the main reason of such fragmented structural analyses.

Several authors have used fluorescence resonance energy transfer (FRET) techniques to study the disposition of the full receptors in the membrane [41–43]. Some donor labels are placed in the protein structure and some acceptor labels in the lipid polar heads, allowing the measurement of the distance between the labeled residues and the lipid bilayer surface. Some set of FRET measurements using a labeled Trastuzumab Fab along with homology modeling techniques allowed Bagossi et al. [44] to propose a structural model for the full ErbB2/Trastuzumab-Fab dimer inserted in the lipid bilayer.

There are only two molecular simulations studies dealing with an EGFR receptor inserted in the membrane. Kastner et al. [41] studied the solvated EGFR tetramer in a lipid bilayer. The study considers the extracellular and transmembrane domains of the receptors summing up to more than 8×10^5 atoms. The multinanosecond simulations (~ 75 ns) were performed using 4,096 processors of the BlueGene supercomputer. Another related system studied by atomistic molecular dynamics simulation is the near half million atom complex simulated over tens of μ s by Shaw's group on the Anton supercomputer, a "hardware" specifically designed to accommodate molecular dynamics algorithms. This system consisted of a complete EGFR dimer including the lipid bilayer [45].

Both studies used massive supercomputer resources which are hardly accessible to the scientific community. The coarse grained (CG) models offer an alternative way to study both larger spatial and time scales of huge biomolecular systems, beyond what is possible with all-atom models (AA), using moderate computational resources [46]. In particular, the Martini force field has been established as a suitable model for the CG description of biological systems [47, 48]. Four atoms per CG particle are mapped in Martini, which offers parameters for several types of molecules including, essentially, lipids and proteins. This model has been successfully used to investigate the structure and dynamics of systems containing lipids and peptides such as transmembrane proteins or antimicrobial peptides [49–51].

Here, we report on the molecular dynamics simulations of the structure and dynamics of the ErbB2 receptor and its interaction with the Trastuzumab monoclonal antibody Fab(mAb) as part of our ongoing project to study, from the experimental and computational points of view, the structure of EGFR/monoclonal antibody complexes [11, 52, 53].

The ErbB2 receptor is studied in monomer and dimer forms, for whose existence experimental evidence has been reported [54, 55]. The dimer associated to receptor overexpressed in cancer cells [55]. Thus, in this manuscript we analyze the capability of the Martini model to perform CG simulation of interaction of a full ErbB2 receptor and Fab-Trastuzumab comparing the results with those obtained by atomistic modeling and also with other experimental data available on similar systems. It should be also pointed out that the simulation of these ErbB2 full receptor systems in its monomeric and dimeric forms, including the lipid bilayer and an antibody Fab has not been ever performed.

Computational methods

Protein–bilayer setup

An atomistic model of the full ErbB2 receptor and the Trastuzumab Fab were taken from the homology structure published by Bagossi et al. [44]. Online resource 1 in the Electronic Supplementary Material section provides the amino acid sequences of the different receptor and the antibody domains used in the present work. The Martini Force Field and its extension to proteins (version 2.2) were used to build the CG topology [47, 48]. Elastic networks (EN) for the CG model of the protein in solution was employed using the ENeDyn method [56].

The application of EN to the whole receptor might introduce undesirable rigidity to the system. The subdomain selection for the EN model is based on the receptor structural characteristics and our previous results on the atomistic ECD. For example, the extracellular subdomains I and III consists of a series of β -sheets which confer a relative rigidity to them. Subdomains II and IV are cystein-rich regions which may be assumed to be also relatively stable in water solution. These assumptions are confirmed by the different ErbBs structures experimentally elucidated either in the staggered or opened conformations simulations [11, 12, 41, 45, 52]. Therefore, the major sources of flexibility may be associated, in principle, with the inter-domain connections. However, a validation of the EN setting procedure was performed by comparison between coarse-grained and atomistic simulations.

Elastic networks between backbone particles were applied separately at each subdomain for the ErbB2 complex and for the Trastuzumab Fab. The parameters controlling the elastic networks were a cutoff radius $R_c = 0.8$ nm and a spring constant $K_{\text{spring}} = 500$ kJ mol $^{-1}$ nm $^{-2}$. We followed the methodology suggested by Periole et al. [56] regarding the selection of parameters for the EN. In the Online resource 2 of the Electronic Supplementary Material, the root mean squared fluctuation (RMSF) values corresponding to the

Table 1 Number of replicas and simulation time for each system

System	# Replicas	Simulation time (μs) ^a
Monomer	3	4
Monomer + Fab	2	4
Dimer	3	4
	1	28
Dimer + Fab	1	4
	1	38

^a Scaled time. See “Computational methods” section for details

ECD are represented for the different combinations of R_c and K_{spring} values compared with the atomistic data. As can be observed the best fit with the atomistic model is obtained with the combination R_c and K_{spring} suggested above.

We have selected the dipalmitoylphosphatidylcholine (DPPC) lipid as a model for the bilayer forming element. Other more complex membrane compositions may exist in the ErbB2 system but these are not clearly defined.

Systems consisting of 1,041–1,052 DPPC molecules solvated in 79,453–80,642 Martini water particles were prepared to build the different lipid bilayers. A triclinic box with Cartesian dimensions $17 \times 17 \times 35$ nm was selected so that periodic image interaction were avoided. The protein was positioned so that the TM helix was inside of the lipid bilayer.

Several replicas were performed for each system. Table 1 collects that number and the simulation time for each one.

Simulation details

All CG molecular dynamics (MD) simulations were performed using the version 4.5.3 of the GROMACS simulation package [57]. An energy minimization using the steepest descent algorithm over 1,000 steps was carried out for the initial structure. Then, a NPT equilibration with position restraints for all protein beads was run for 40 ns, and finally, a NPT equilibration without position restraints was run for 8 ns.

The particle mesh Ewald (PME) method [58] was used to calculate long-range electrostatic interactions, using a maximum grid spacing of 2.5 Å, fourth-order (cubic) interpolation for the fast Fourier transforms and a relative dielectric constant of 15. A dielectric constant of 15 is used for explicit screening to balance the increased hydration strength of many of the CG particle types [47]. The temperature was kept constant at 310 K by coupling the protein and the solvent independently to an external bath using the Berendsen algorithm with a coupling constant of 1 ps [59]. Isotropic scaling was used for the pressure (1 bar) with a coupling constant of 2.0 ps and a compressibility of 3.5×10^{-5} bar⁻¹ following the Berendsen algorithm [59]. The temperature range used in the original Martini force field parameterization for lipids was

270–330 K. The calculated transition temperature for DPPC is 295.5 K below the experimental value of 315 K [47]. Therefore, the 310 K temperature selected for our simulations could be considered physiologically relevant.

The dynamics were integrated using the velocity Verlet integrator, with a time step of 20 fs and bonds constrained using the LINCS algorithm [60]. Thus, production dynamics were performed at constant pressure and temperature (NPT ensemble) storing the trajectory every 0.5 ns to increase the statistical significance. Independent trajectories were generated for each studied model using different seed numbers for the initial velocity assignment.

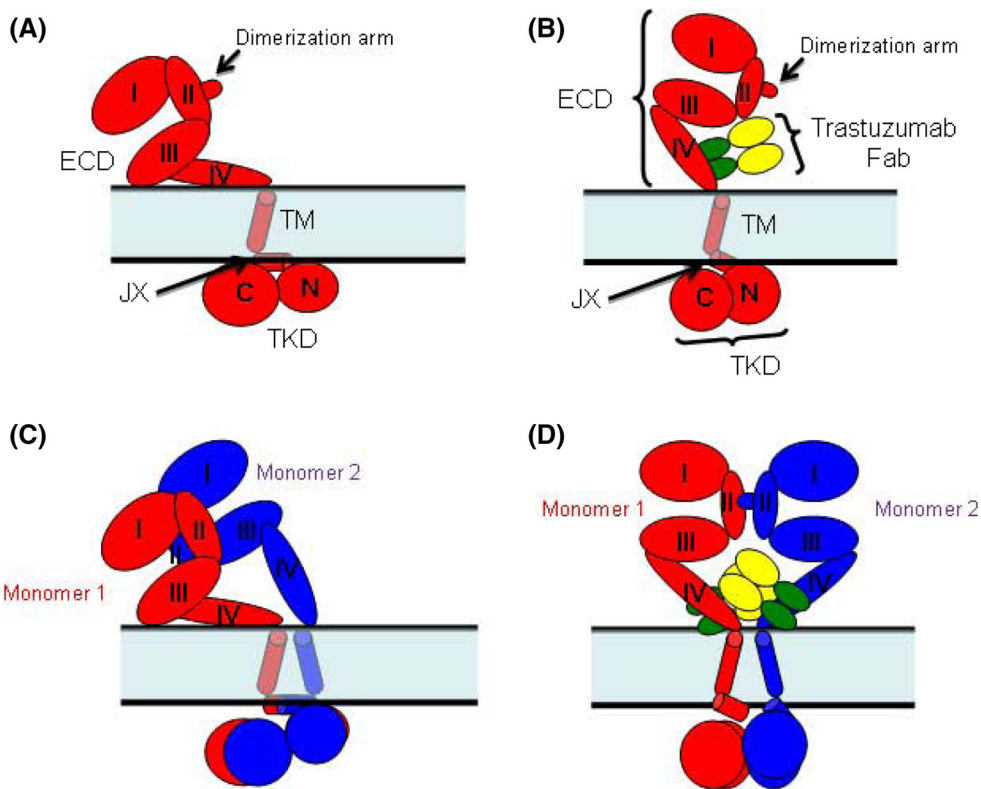
It has been proposed that the time unit used in CG simulations using the Martini force field should be multiplied by four to obtain an estimation of the corresponding atomistic time unit [61]. This conversion factor is derived from the diffusion dynamics of CG water compared to atomistic water. Therefore, the dynamic properties analyzed through the results section are reported in the scaled time units.

Distance maps between the backbone particles were calculated in order to analyze the interdomain interactions. Normalized maps were constructed by counting the number of frames where the inter residue backbone particle distance is below a threshold of 0.7 nm and dividing by the total number of frames. Thus, a value of one in the distance map would corresponds to a persistent distance below 0.7 nm between the corresponding residue backbone particles along the whole trajectory.

Principal component analysis (PCA) [62, 63] is a method that takes the trajectory of long MD simulations and calculates the dominant modes in the molecular. Thus, the configurational space is reduced, containing few relevant collective degrees of freedom in which long range fluctuation can be studied. A PCA diagonalizes the covariance matrix of the atom fluctuations from their average trajectory. In this framework, the larger eigenvalues correspond to eigenvectors which explain most of the variance associated to particle fluctuations. The eigenvalue ordering allows to identify a small set of modes that capture most of the fluctuations. We have performed a PCA analysis in order to identify the lowest frequency motions occurring in the tyrosin-kinase dimer. The g_covar and g_anaeig tools in the GROMACS package were used to perform the PCA analysis.

Results and discussion

CG simulations were performed on both the monomer and dimer forms of the ErbB2 receptor in a bilayer model. The complexes with the Trastuzumab Fab bound to its corresponding epitope at the ECD are modeled in order to study the antibody effect on the structure and dynamics of the receptor. Scheme 1 depicts both the Trastuzumab Fab



Scheme 1 **a** Schematic of the antibody-free ErbB2 monomer receptor. The subdomains I, II, III and IV of the extracellular domain (ECD), the transmembrane (TM), the intramolecular juxtapamembrane (JX) and the tyrosin kinase (TKD) are shown in red. The C and N label stands for the C-lobe and N-lobe domains of the TKD. The shadow area represents the lipid bilayer. **b** Schematic of the antibody-bound ErbB2 monomer receptor. The Trastuzumab Fab (antibody) is

antibody bound to the ECD of the monomer and dimer forms of the full ErbB2 receptor embedded in a lipidic bilayer membrane model.

In what follows, the structure and dynamics of the ECD, TM and TKD domains will be separately discussed for both the monomeric and dimeric forms without and with trastuzumab bound to the ECD, respectively. A comparison with other available atomistic simulation models as well as with experimental data will be done, whichever is possible, in order to evaluate the performance of the CG models. Finally, we make a discussion of all results.

Extracellular domain

Monomeric form without and with trastuzumab

Selected initial and final snapshots of the monomer simulations without (antibody-free) and with (antibody-bound) trastuzumab are depicted in Fig. 1. Firstly, in the antibody-free monomer system the ECD presents a hinge movement at the interface of subdomains III and IV (residues 460–480) that approaches subdomain IV to the

bound to the subdomain IV of the ErbB2 receptor. The variable (VD) and constant (CD) domains are shown in green and yellow colors respectively. **c** Schematic of the antibody-free ErbB2 homodimer and **d** schematic of the antibody-bound ErbB2 homodimer, the two antibodies bound to their respective subdomains IV are shown with the same color code as in **b**

dimerization arm (subdomain II). Figure 2 shows the first eigenvector of the PCA analysis performed on simulations of both monomeric systems. A remarkable similarity can be observed to the result obtained with the PCA analysis performed on atomistic simulations of ErbB2 ECD (see, for example, Figure 4 of Ref. [52]). This movement in the CG simulations agrees also with previous atomistic simulations performed on the monomeric ErbB2 extracellular domain [11, 12]. Remarkably, a similar motion has been recently described by molecular dynamics simulations of the full EGFR receptors with and without ligand [45]. This structure has not been yet reported by crystallographic techniques likely due to the rigid packing of the produced crystals [11]. Thus, the CG model reproduces the intrinsic flexibility of the extracellular domain observed in atomistic simulations. Furthermore, the presence of the membrane does not seem to hinder this intrinsic flexibility of the ECD.

A closer comparison with the atomistic simulations can be seen in Fig. 3. This shows the root mean squared fluctuation (RMSF) analysis of the residues in the ECD domain for both the CG and atomistic simulations of the monomer taking as a reference the Bagossi's structure [44]. The plot compares the

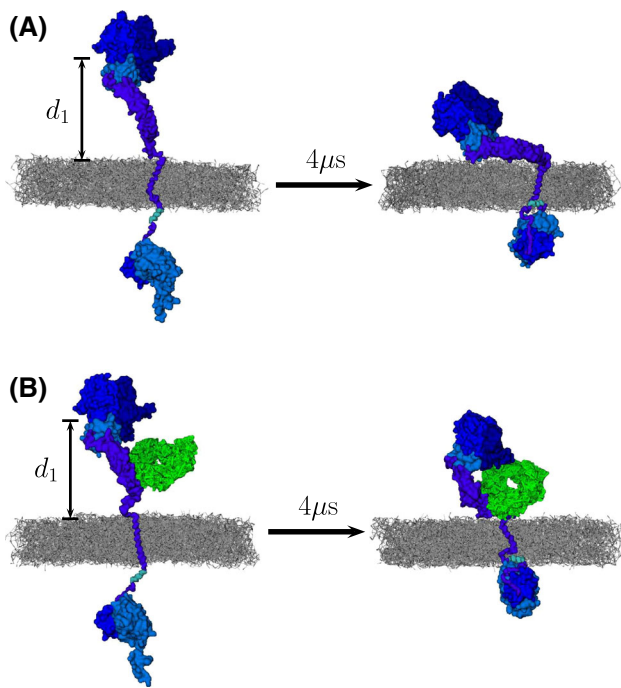


Fig. 1 Initial and final conformations of a selected replica of **a** the antibody free ErbB2 monomer and **b** the antibody-bound ErbB2 monomer. ErbB2 receptor and antibody are shown in blue and green, respectively. Space fill representation for the CG particles. Lipid bilayer molecules are depicted as gray lines and water particles are omitted. The distance d_1 is defined to measure the approach of the receptor to the lipid bilayer (see text for details). The initial conformations of the ErbB2 monomer were prepared using the Bagossi's structure

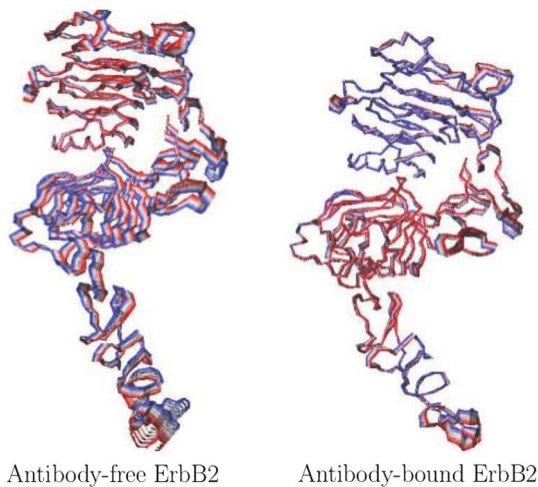


Fig. 2 First PCA eigenvector for the ErbB2 ECD monomer corresponding to the antibody-free (*left*) and antibody-bound (*right*) systems. Only the backbone is represented (as connecting lines). Several projections of the backbone are plotted between the two extremes denoted with red and blue colors

fluctuation values for the C_α in the atomistic models against the backbone particles of the CG particles (mapped in the C_α atoms in Martini). In spite of the elastic networks treatment

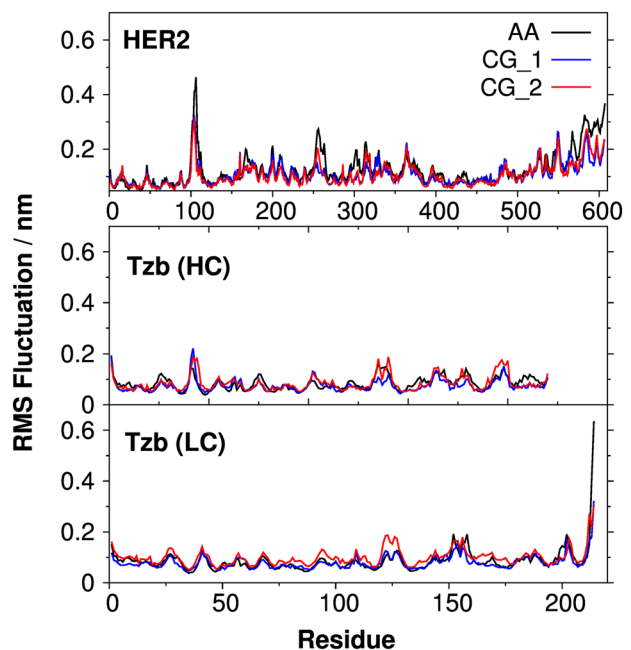


Fig. 3 RMSF plots for the ErbB2 ECD (*top*), Fab-trastuzumab heavy chain (HC, *middle*) and light chain (LC, *bottom*). The atomistic simulations were performed on the antibody-bound ErbB2 ECD in water11. The CG_1 and CG_2 labels correspond to two independent CG MD simulations. The reference structure in all cases was taken from the Bagossi's structure

of the CG model (see details in “Computational methods” section), which is expected to reduce fluctuation values, the profile is rather similar in both cases, showing higher values in the loops and in the subdomains involved in the hinge motion above mentioned.

The binding region between the ErbB2 extracellular epitope (subdomain IV) and the Variable Domains of both the Heavy (V_H) and the Light Chain (V_L) of the monoclonal antibody has been experimentally characterized by three ErbB2 loops. Loops formed by residues 557–561 and 593–603 are mainly electrostatic, whereas the 570–573 loop makes principally hydrophobic contacts with the V_H of the antibody. Figure 4 shows the distance maps of the contact interface between the subdomain IV and the antibody variable domain for the crystal, atomistic and the CG structures, respectively. As it can be seen, the variable domain of the monoclonal antibody structure maintains its interactions with the ErbB2 extracellular epitope (subdomain IV) in all CG replicas as compared to the experimental structure (PDB code: 1N8Z) [10]. Furthermore, a hinge movement is also observed in this case, which favours the interaction of the antibody constant domain with the dimerization arm in subdomain II. Thus, residues Thr256–Pro263 at the dimerization arm are found at distances below 0.7 nm from Fab residues Ser120–Gly125

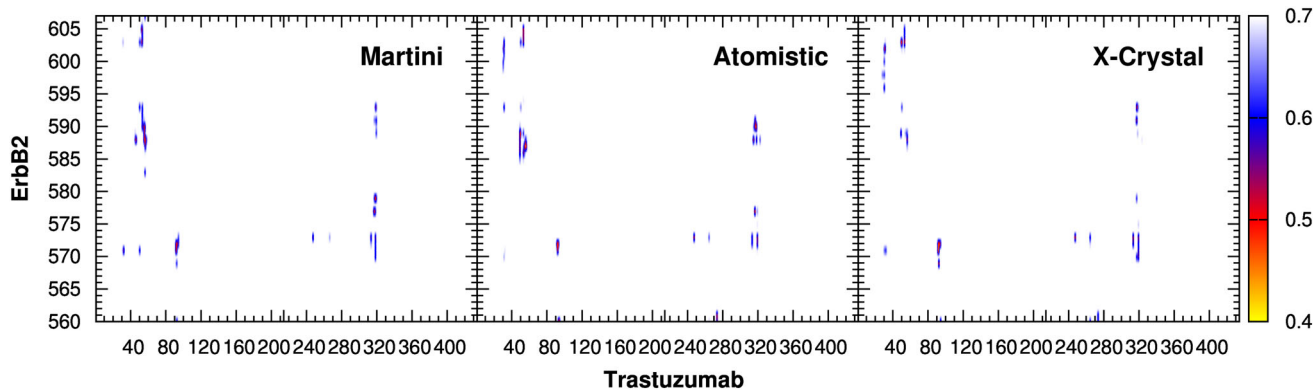


Fig. 4 Distance matrix between residue pairs of the ErbB2 subdomain IV and the variable domain (VD) of the antibody monomer. The distance corresponds to the smallest distance between the CG-beads

of two residues in the receptor and in the antibody, respectively. A cut-off distance of 0.7 nm was used. The experimental structure (PDB code: 1N8Z) was mapped on the MARTINI CG model

and Ser210–Asn211 in the Heavy Chain (HC), in line with the interactions reported for the atomistic simulations [11].

Along the manuscript, the comparison with the atomistic model was described using the ECD from the full-receptor structure (Figs. 3, 4). A more appropriate comparison should be made with the CG model of the ECD alone-trastuzumab complex. This work will be described in more detail in a forthcoming paper, though, some representative results are described below. The comparison of RMSF plots that was discussed when answering the EN question is itself a source of validation of the coarse-grained model. Another source of validation regarding the protein–protein interactions are the distance matrices evaluated between the ECD epitope and its interaction with the Trastuzumab Fab. In the Online resource 3 of the Electronic Supplementary Material section, the distance matrices calculated on the atomistic and coarse-grained models for the ECD and trastuzumab complex are shown. It can be observed that most of the crystallographic contacts are well preserved in the atomistic case as well as in the Martini model.

A third validation test contemplates the dynamic properties of the system. A comparative PCA analysis of the atomistic and CG simulations following the method proposed by Siuda and Thogersen [64] was carried out. The eigenvectors found when diagonalizing the covariance matrix were then used in the root mean-square inner-product (RMSIP) analysis (see equation 1 of [64]). This analysis quantifies the overlap between the essential subspaces (described by the 10 first eigenvectors) obtained from the AA and CG simulations. The RMSIP obtained was 0.51, which may be considered satisfactory as is suggested by Siuda and Thogersen [64].

In Fig. 5, it is shown two snapshots corresponding to a fitting between the backbone CG particles and the C_α atoms of the atomistic model for the ECD/antibody complex. A root mean square deviation (RMSD) value of 0.8 nm was obtained for the full complex, whereas the RMSD values

calculated separately for each constituent were 0.4 nm for the ECD chain and 0.3 for the Trastuzumab Fab. In this figure, it can be also observed the additional interaction between the antibody constant domain and the ErbB2 dimerization arm that has been captured similarly by both atomistic and CG simulations.

As it can be seen in Fig. 1, the final configurations of the protein with respect to the lipid bilayer are rather different in the free and bound-antibody monomer forms. In all replicas of the free-antibody monomer, an approach of the protein to the lipid bilayer surface is observed. On the contrary, this approach has not been detected in the case of bound-antibody complexes. In our simulations, the vertical distance between the lipid polar head particles and the backbone center of mass (COM) corresponding to subdomains I, II and III was evaluated to quantify the approach of the ectodomain to the bilayer surface (d_1 in Fig. 1). Indeed, in the monomer systems, the calculated distance d_1 drops from the initial 10.5 nm to final values around 4.0 ± 0.3 and 7.9 ± 0.3 nm for the free and the bound-antibody monomer forms, respectively. The approach of the free-bound antibody monomer is in agreement with some FRET experiments for the homolog EGF-ErbB1 homodimer where no antibody is present. [42, 43, 65] In those experiments, it has been shown that the ErbB1 ectodomain lies parallel to the cell membrane at distances around 4.0 nm. The geometric parameter used in the FRET experiments for the homolog ErbB1 (EGFR) receptor is the distance between a labelled epidermal growth factor (EGF) ligand bound to the ErbB1 receptor and the bilayer surface, which is comparable to the d_1 distance for our system defined above. These authors have proposed that this approach of the receptor to the membrane is caused by the high flexibility of the domain IV in the ECD. Anyhow, the antibody bound to the domain IV is also anchored to the bilayer membranes (see final state in Fig. 1b), which in our models does not allow the approach of the receptor to the membrane in the case of the bound-antibody monomer.

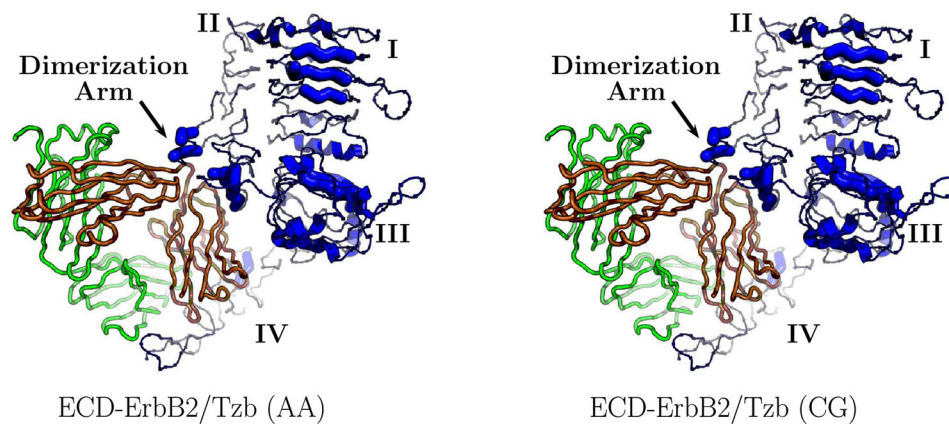


Fig. 5 ErbB2 extracellular domain in complex with the Trastuzumab Fab showing the interaction between the dimerization arm and the antibody constant domain (arrows). *Left* atomistic model [ECD-mAb(AA)]. *Right* CG model [ECD-mAb(CG)]. The two Fab chains

are depicted in green and brown colours. Roman numbers indicate the location of the subdomains in the ErbB2 receptor. The ECD-mAb (CG) was extracted from the full receptor simulation

The final structures corresponding to the antibody-free monomer present persistent interactions between residues 359–364 and 393–397 of the subdomain III, residues 481–484 and 611–620 of subdomain IV and the bilayer surface. These fragments contain several negatively charged ASP and GLU amino acids able to interact with the positively charged lipid choline heads of the bilayer. In the antibody-bound monomer case, the trastuzumab is able to develop permanent interactions with the bilayer surface, as above mentioned, hindering the approach process of the receptor to the lipid bilayer. The closest residues of the antibody to the bilayer surface are Gly16, Asp17, Arg18 and Ser76 located at the heavy chain of the Fab.

Several replicas of the simulated systems were performed as stated in Table 1. As it might be expected all replicas do not behave identically. A brief discussion about variance across replicas has been added, for the interested reader, as Online resource 4 in the Electronic Supplementary Material section.

Dimeric (homodimer) form with and without trastuzumab

The antibody-free ECD dimer structure (Scheme 1c) is mainly driven by the interaction between the dimerization arms at the subdomain II of each monomer. The overall interaction through the dimerization arms originally found in the crystallographic structures of the ErbB1 ECD [66] and subsequently used by Bagossi for his ErbB2 model [44] is preserved along the CG simulations. However, some weakening of the dimer interaction appears in the antibody-bound dimer model (Scheme 1d). Figure 6 presents the normalized residue contact maps for subdomain II–subdomain II complex interface for the antibody-free and antibody-bound models, respectively. It can be observed that

the residue contacts in regions a and b are weakened in the antibody-bound dimer model. Furthermore, the interaction in the subdomain II C-terminal region (residues 306–309 in region c) has disappeared in the antibody-bound case. Thus, the proximity of the constant domain of the antibody disturbs the loops at subdomain II connecting the dimeric interface. The variable domain of the antibody structure maintains its interaction with the ErbB2 extracellular epitope (subdomain IV). The trastuzumab-subdomain IV interaction observed in the monomer is rather similar to that found in “Monomer 1” of the ErbB2 dimer (see Fig. 7). The other ErbB2 “Monomer 2” presents a somewhat different interaction pattern with trastuzumab. Online resource 5 in the Electronic Supplementary Material section shows the distance matrices for the two monomers corresponding to the longest replica of the trastuzumab-bound homodimer system. The matrix labelled “Monomer 1” corresponds to the monomer lying on the bilayer surface (see Fig. 7). This matrix is essentially similar to that described for the monomer case (see Fig. 4) and comparable to the crystallographic structure. The matrix labelled “Monomer 2” corresponds to the monomer standing upright. The residues involved in the ECD epitope–trastuzumab interaction are maintained. However, a different distance matrix pattern is obtained concerning residues 560–565 and 586–593 of the ErbB2 chain (see areas labeled “c” and “b” in the Monomer 2 map). The first of those two aminoacid sets (residues 560–565) are in the N-terminal fragment of subdomain IV near the loops connecting to subdomain III. It is worth noting that in the same trastuzumab-bound system, a disruption of the dimerization in the C-terminal fragment of subdomain II was described (see labeled area “c” in Fig. 6). Therefore, it can be assumed that the Fab bound to Monomer 2 may be

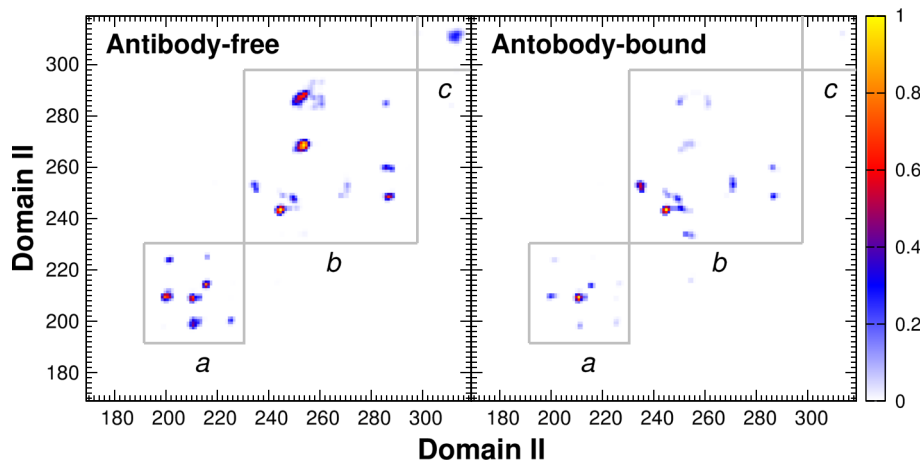


Fig. 6 Normalized contact maps for subdomain II–subdomain II interaction between both monomers in the antibody-free (*a*) and the antibody-bound (*b*) ErbB2 dimers. This map is constructed by counting the number of frames where the inter residue backbone particles distance is below a threshold of 0.9 nm and dividing by the

total number of frames. Lowercase letters stand for the different regions of contact between dimerization arms. The color scale is in the range of 0 (no interaction along the trajectory) to 1 (full interaction along the trajectory)

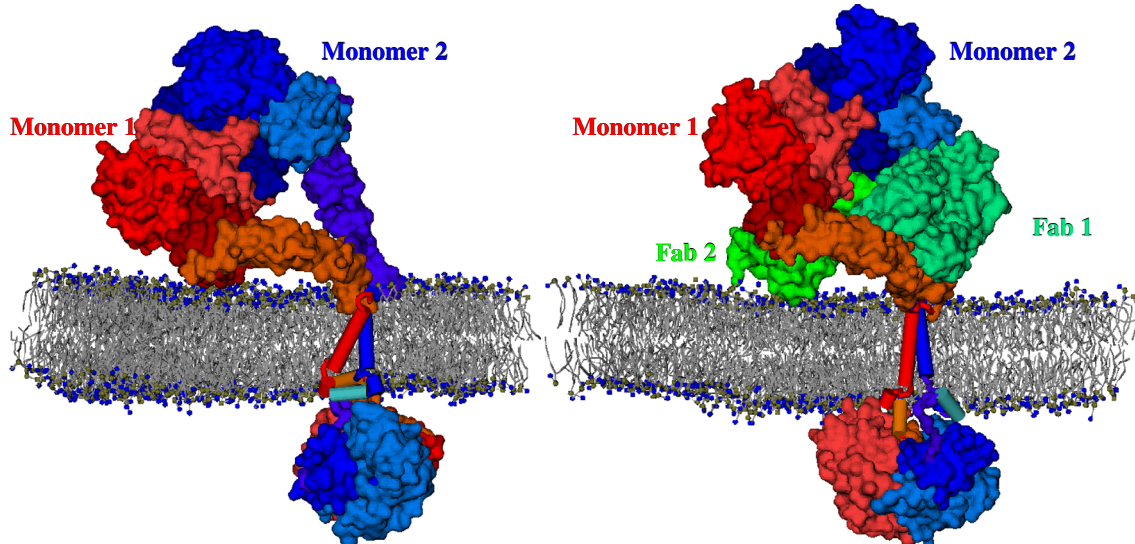


Fig. 7 Full antibody-free (left) and antibody-bound (right) ErbB2 homodimer structures at the end of the simulation. Space fill representation of the dimeric structures of ErbB2 are shown in red (Monomer 1) and blue (Monomer 2) for each monomer. On the other

hand, the antibody (Trastuzumab) is represented in green. Lipid bilayer molecules are depicted as gray lines. Water particles are omitted for clarity

responsible for the loose interface in the subdomain II dimerization region.

The C-terminal fragment of subdomain IV is another structural characteristic of the ECD dimer structure. Atomistic scale simulations performed on ErbB2–ErbB3 ECD dimers in solution show a clear interaction between the C-terminal segments of the subdomains IV [52]. This is also the situation exhibited by some crystallographic structures of homolog receptors, e.g., the ErbB1 ECD dimer [66]. The CG simulations of the antibody-free dimer system show the expected subdomain IV C-terminal interaction between the

two ErbB2 monomers. The contact map associated to subdomains IV for both monomers presents a remarkable interaction between the C-terminal fragments in the antibody-free system. These contacts disappear in the antibody-bound dimer complex (see Online resource 6). Thus, the antibody bound in the vicinity of subdomain IV exerts a hindering effect on the association of these subdomains at their respective C-terminal fragments located above the membrane surface.

In Fig. 7, the final conformation of the antibody-free (Fig. 7a) and antibody-bound (Fig. 7b) homodimer

systems are shown from one of the simulation. It can be observed that for the antibody-free homodimer, one of the ErbB2 ECD monomer lies on the bilayer surface (Monomer 2 in Fig. 7a) whereas the other monomer remains in a more upright position (Monomer 1 in Fig. 7a). The measured distances from the ECD COM to the bilayer surface, as defined in the previous section, reach a plateau with values of 7.8 ± 0.3 and 4.0 ± 0.3 nm for Monomer 1 and 2, respectively. These values agree with the FRET measurements reported on the ErbB1 receptor [42, 43, 65] and shown in the previous section. In the system containing trastuzumab, the presence of the antibody hinders in some way the approach of any of the ErbB2 ECD segments to the membrane (see Fig. 7b). In analogy to what is observed in the antibody free case, one monomer approaches the bilayer surface more than the other, keeping distances from both ECD to the lipid layer of 5.5 and 8.5 nm for the labeled Monomer 1 and 2 in Fig. 7b, respectively. These distances are larger than the corresponding to the antibody-free system due to the interposition of the antibody between the bilayer and the ErbB2 receptors.

A comparative analysis of these results with atomistic models reported for the ErbB1 dimer can be done. The ECD ErbB1 dimer model described in Refs. [41, 45] for the active forms is very similar to our CG model. The interaction between the C-terminal fragments of both subdomains IV is a weakly crossing interface so that the N-terminal portions of the transmembrane domains can be close. The inactive form described in Ref. [45] shows both C-terminal fragments far enough to avoid the interaction between the N-terminal transmembrane segments. The trastuzumab effect is to weaken the subdomain IV interaction, giving rise to a distortion of the transmembrane domain association. The relative orientation of the ECD domains to the bilayer surface may be driven by the electrostatic properties of the lipid polar heads. In Ref. [41] the lipid molecules are zwitterionic and the active ErbB1 ECD domains lay down on the lipid bilayer. The same ECD domains remain in an upright position when a mixture of zwitterionic and charged lipids is considered [45]. Our CG models, which takes into account zwitterionic lipids, shows a similar behavior to the active ErbB1 system described in Ref. [41]. We also found one monomer that is closer to the bilayer surface than the other. A more detailed discussion about the relative disposition of the ECD domains with respect to the lipid bilayer has been provided above.

Transmembrane domain

The dimeric association of transmembrane domains has been related to play a role in the activation of the entire receptor [20, 67]. In this section we describe the results obtained on the transmembrane association of the homodimer systems from CG simulations.

The starting structures for the simulations, which come from the Bagossi's model, present the transmembrane fragments interacting mainly through the N-terminal and central sections of each chain, namely, residues ARG625–LEU640. This arrangement of the TM dimer is maintained along the simulations. Figure 8 shows contact maps for the residues belonging to the transmembrane domains collected during the last μ s of the antibody-free (Fig. 8a) and antibody-bound (Fig. 8b) homodimers.

Firstly, the contact maps of the antibody-free homodimer are in agreement with the TM helix packing interface reported for the ErbB2 dimer by Bocharov based on NMR experiments (PBD code: 2JWA) [20] as follows: these authors hypothesized that the arrangement experimentally elucidated would correspond to an active form of the TM dimer. The dimer is favoured by the interaction between a tandem variant of GxxG-like motifs located at the N-terminal section (see Figure 2F of Ref. [20]). Our CG simulations arrive to a homolog interaction tandem corresponding to residues Ser627–xxx–Phe631–xxx–Thr635–xxx–Val639 (see Fig. 8). In addition, The contact maps are also very similar to those reported by Arkhipov et al. [45] for the homolog EGFR dimer in the disposition associated to an active form of the complex (see Fig. 4 of their paper).

On the other hand, the system containing the antibody develops additional interactions between amino acids located close to the C-term region of the TM, which are not seen for the antibody-free case (please compare Fig. 8a, b). It can also be observed that in the antibody containing system, a transmembrane helix is displaced asymmetrically with respect to the other one (see Fig. 9). This unsymmetrical arrangement is depicted in the contact map by the off-diagonal marks near the N-terminal section (residues Pro620 and Ala626, see Fig. 8b). It can also be observed a four residue displacement of the interaction tandem towards the TM C-terminal part (THR630–X₃–ALA634–X₃–GLY638–X₃–PHE642 [see Fig. 8]).

Juxtamembrane (JX) intracellular domain

The juxtamembrane (JX) domain (residues Lys659–Leu669), which is located between the transmembrane and kinase domains, is related to important regulatory functions such as regulation of the receptor trafficking and inactivation [68]. Thus, the arrangement of this JX domain with respect to the bilayer and to the TKD has been studied and related to regulatory functions of the EGFR family. In this section, we define the torsion angle (ϕ) between the JX α -helix axes as well as the θ angles between these axes and the bilayer surface, both shown in Fig. 10. Those definitions help to quantify the JX spatial arrangement.

Fig. 8 Normalized contact maps of the transmembrane (TM) interaction for the antibody-free (**a**) and antibody-bound (**b**) ErbB2 homodimers. The scale represents the occupancy of the interaction along the analyzed trajectory. See “Computational methods” section for details of how the contact map is calculated. The tandem makes reference to the GxxG-like motifs along the chain

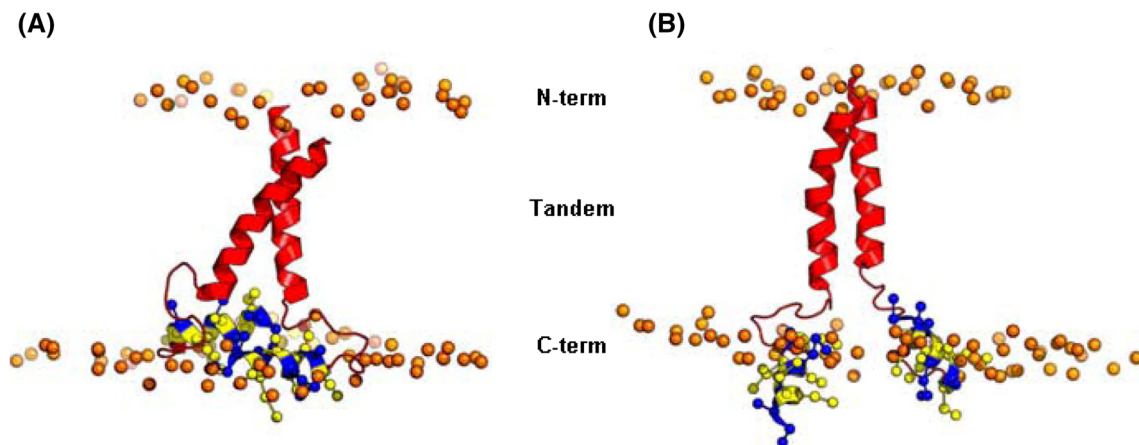
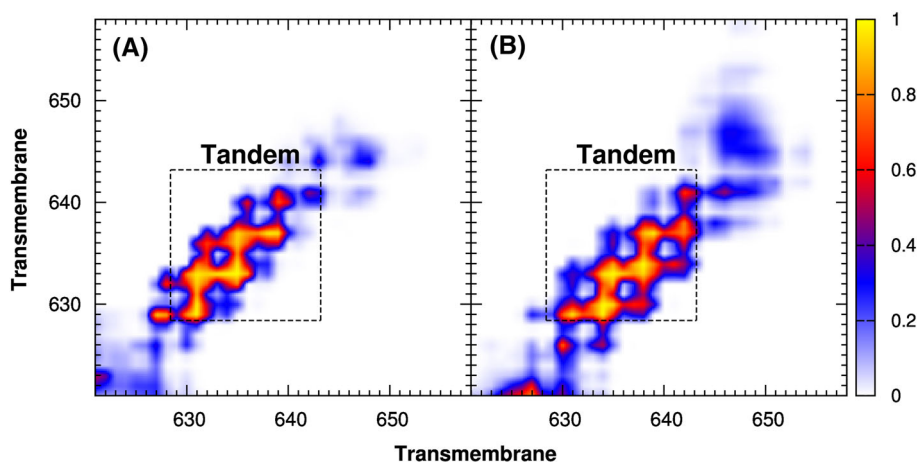


Fig. 9 Cartoon representation of the transmembrane (red) and juxtamembrane (blue) fragments extracted from the final snapshot of the **a** antibody-free and **b** antibody-bound ErbB2 dimer simulations. The lateral chains of the juxtamembrane domain are shown as

blue and yellow CPK balls for the charged and hydrophobic residues, respectively. Lipid polar head particles are represented as red CPK balls. Water and the most lipid atoms are omitted to gain clarity in the figure

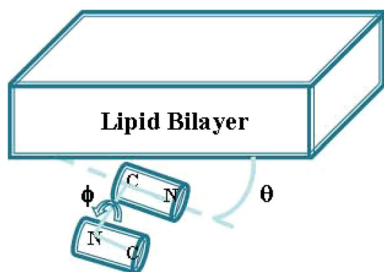


Fig. 10 Schematic representation of the mutual disposition of the juxtamembrane (JX) fragments (cylinders) and the lipid bilayer (prism). The θ angle gives an idea of the position of the JX domain respect to the lipid bilayer whereas the ϕ angle shows the relative orientation of the JX domains in the case of the homodimer complex (see definition of these angles in the text)

Monomeric form without and with trastuzumab

In the monomer case, it can be observed that the JX segment adopts a parallel configuration with respect to the

bilayer surface so that the polar residues are oriented to the water phase whereas their hydrophobic amino acids face the lipid interior. This observation agrees with the NMR experimental results obtained on the EGFR JX fragment [69]. The angle (θ) formed by the JX helix axis and the lipid bilayer surface is similar for both cases (19 ± 2 for the unbound ErbB2 and 21 ± 2 for the mAb complex).

Dimeric (homodimer) form with and without trastuzumab

The antibody-free homodimer reach an antiparallel arrangement of both JX α -helices ($\phi \sim 7^\circ$, see Table 2) as well as a parallel disposition with respect to the bilayer surface ($\theta \sim 3^\circ$ and 7° , see Table 2). It can be noted that the antiparallel disposition has been identified to be essential for an active dimer conformation. [45, 67] On the other hand, it can be observed a severe distortion of the JX antiparallel arrangement in the antibody-bound homodimer

Table 2 Geometrical parameters of the juxtamembrane arrangement

System	Torsion φ (°)	Angle θ (°)	
		Monomer 1	Monomer 2
Antibody-free monomer	n.a	19 ± 2	n.a
Antibody-bound monomer	n.a	21 ± 2	n.a
Antibody-free dimer	7 ± 5	7 ± 3	3 ± 2
Antibody-bound dimer	57 ± 9	27 ± 4	60 ± 3

n.a not applicable

system ($\varphi \sim 57^\circ$, see Table 2). In the same way, the parallel alignment respect to the bilayer surface is lost ($\theta \sim 27^\circ$ and 60° , see Table 2).

Besides the parallelism with the bilayer exhibited by the JX segments in the antibody-free simulations, these fragments remain anchored on the surface of the membrane, as can be observed in Fig. 9. The hydrophobic residues Ile660, Tyr663, Met665, Leu668 and Leu669 (yellow CPK balls in Fig. 9) face the lipid acyl tails whereas the Lys and Arg charged amino acids (blue CPK balls in Fig. 9) interact with the lipid polar heads. This picture of the interaction between the JX fragment and the lipid bilayer are in agreement with the NMR results [68] and with the description recently provided for the EGFR dimer [45, 67] in its active conformation. In the case of the antibody-bound homodimer almost all these interactions are weakened, losing the antiparallel arrangement of both JX α -helices.

TKD intracellular domain

Regarding the TKD, the general observation in all the systems is that the TKD approaches the lipid bilayer surface on the intracellular side.

In the monomer cases, the distance from the tyrosin-kinase COM to the bilayer surface is 2.6 ± 0.2 nm for both systems. The tyrosin-kinase residues at distances to the membrane surface smaller than 0.8 nm to the membrane surface correspond to the residues Ile850–Gly859, Leu873–Arg875 and Asp940–Cys943.

The representation for the dimer structures in Fig. 7 apparently shows a closer approach of the TKD dimer to the bilayer surface in the case of the antibody-bound ErbB2 homodimer. Looking at the distances between the TKD-COM and the bilayer surface, averaged over the last μ s of all the corresponding replicas, the cytoplasmic domains of the antibody containing system present a slightly closer approach to the membrane surface (2.8 ± 0.2 nm) than the antibody-free dimer case (3.0 ± 0.2 nm). Online resource 7 in the Electronic Supplementary Material collects the

plots of the distance between the TKD COM and the bilayer surface along the simulation time for several replicas of the trastuzumab-free homodimer system. The approach to the bilayer surface occurs in the first microsecond reaching a distance between both TKDs COM to the bilayer surface that fluctuates between 2.5 and 3 nm, as illustrated in that online resource.

Figure 11 depicts the disposition of the TKD dimer relative to the bilayer surface. The residues nearer to the lipid polar head particles are highlighted in yellow. There are three groups of residues that permanently approach the bilayer surface at distances below 0.8 nm, namely, Gly850–Lys859, Leu873–Arg875 and Trp937–Cys943 located in the C-lobe of the kinase domain. The first and third fragments contain charged residues able to interact with the lipid polar head particles. This result is in line with the X-ray elucidated structure of the TKD ErbB1 dimer complexed with a lipid-like molecule [68]. It can also be observed in each case that the TKD dimer approaches the bilayer unsymmetrically, being one monomer closer to the bilayer surface. This result is in close agreement with the full atomistic models of the EGFR dimer in a lipid bilayer [45].

The interaction between both tyrosin-kinase domains corresponds to the back-to-back configuration as was proposed in the original Bagossi representation. The N-lobe of one chain interacts with the C-lobe of the other, leaving the active site in the opposite sides of the contact surface formed by the N–C–C–N interaction of both TKDs (see Fig. 11). As the dynamics evolves, the back to back interaction is continuously lost due to a progressive disruption of one of the two N-lobe C-lobe interactions. In order to examine the opening movement of the tyrosin-kinase dimer, we performed a Principal Components Analysis (PCA) on the last μ s of the trajectory focusing on the backbone particles of the tyrosin-kinase domain. The first eigenvector extracted from the fluctuation analysis shows the increased displacement of one tyrosin-kinase C-lobe with respect to the N-lobe belonging to the other ErbB2 tyrosin-kinase chain. Figure 12 depicts a schematic representation of the main PCA component corresponding to the Trastuzumab-free system. Several projections of the backbone are shown in different colors between the two extreme points (blue and red colors) to illustrate the displacement of one C-lobe out of its N-lobe partner.

The influence of the Trastuzumab Fab in the TKD dimer interface seems to be rather subtle as can be deduced from the simulations reported in this work. Figure 13 presents the evolution of the COM distance between the N and C lobes of the two monomers (part a) and from those to the bilayer surface (part b).

On one hand, one of the two interacting N-lobe C-lobe pairs in the TKD dimer is weakened at some point. As can

Fig. 11 Cartoon representation of the tyrosin-kinase domains extracted from the final snapshot of the **a** antibody-free and **b** antibody-bound ErbB2 dimer simulations. *Upper*: relative position of the TKD dimer respect to the bilayer. Lipid polar head particles are represented as red balls. Lower: TKD dimer image taken from the normal to the bilayer viewpoint. Lipid particles are omitted. The N and C lobes are shown for one of the chains to illustrate the back-to-back arrangement. Magenta shadow surfaces correspond to residues involved in the active site

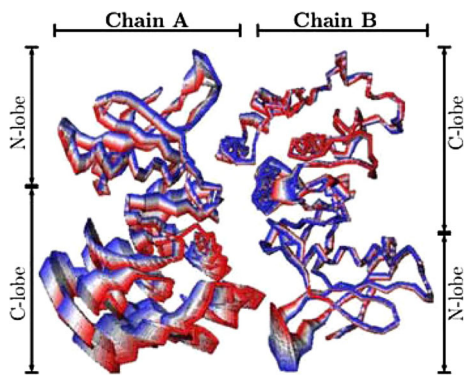
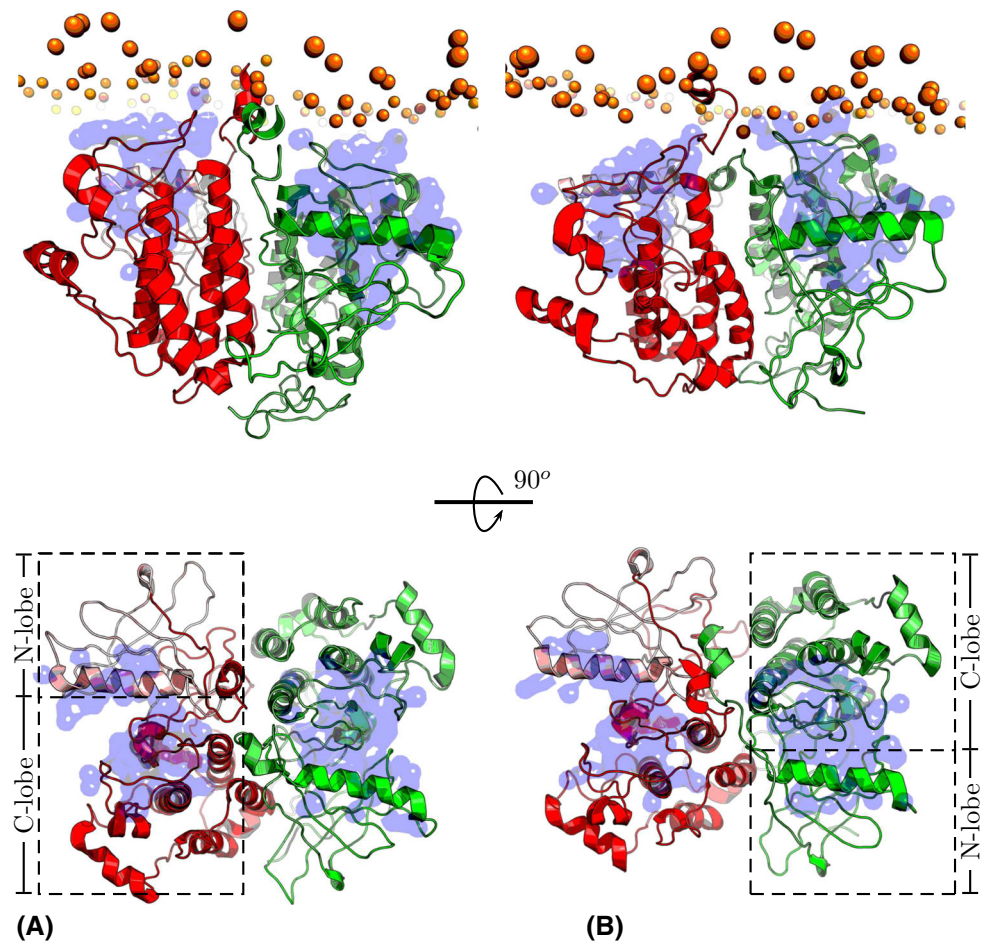


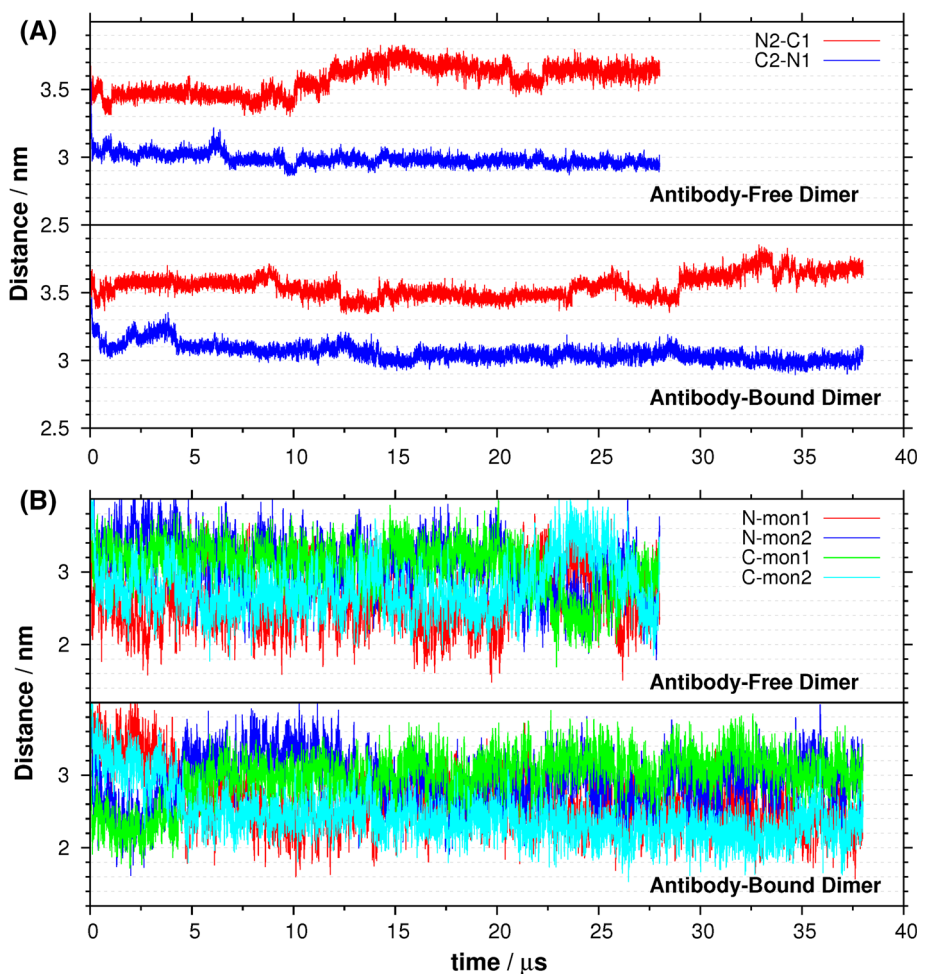
Fig. 12 First PCA eigenvector for the tyrosin-kinase dimer. Only the backbone is represented (as connecting lines). Several projections of the backbone are plotted between the two extremes denoted with red and blue colors

be observed in Fig. 13a, the inter-COM distance between the Monomer 1 C-lobe and Monomer 2 N-lobe is elongated to values above 3.5 nm whereas the equivalent distance between Monomer 1 N-lobe and Monomer 2 C-lobe remains around 3 nm. The evolution is similar in the trastuzumab-free and bound cases as well. This is in

agreement with the essential dynamics analysis discussed above where an analogous opening was reported.

On the other hand, the relative position of the TKD dimer respect to the bilayer surface shows some features already discussed in the monomer case. Each TKD chain shows one lobe closer to the bilayer than the other. Any of the lobes N or C can alternate the approach to the bilayer surface (see for example the red and green lines in part b graphs of Fig. 13). The interchain N lobe–C lobe interaction is revealed by the superposition of red (N lobe Monomer 1) and cyan (C lobe Monomer 2) curves on one side and blue (N lobe Monomer 2) and green (C lobe Monomer 1) lines on the other. The interaction pair formed by the N lobe in Monomer 2 and the C lobe in Monomer 1 seems to be systematically farther from the membrane surface than the other N lobe–C lobe interaction. This observation correlates with the distance elongation shown by Monomer 1 C-lobe and Monomer 2 N-lobe interaction. Finally, a subtle observation regarding the effect of the antibody can be the slightly lower overall distance between the TKD dimer to the bilayer surface as can be deduced from the plots in part B (points in the antibody-bound case plot

Fig. 13 **a** Distances between the COM of N and C lobes in the TKD dimer interface. **b** Distances from the TKD dimer N and C lobes to the bilayer surface



reach distance values lower than 2 nm more frequently than in the antibody-free case).

The TKD is marginally modified respect to the initial model proposed by Bagossi. Due to the Elastic Networks treatment, no conformational changes in the active site are contemplated and a comparison with simulations of the TKD cannot be performed at the moment. The TKD dimerization is stable in its initial conformation although some trend to an asymmetric disposition of the C–N lobes can be depicted from the PCA analysis performed on the particle dynamics fluctuations. An extrapolation of this movement will presumably drive to an asymmetric configuration of the tyrosin-kinase dimer with only an N-lobe/C-lobe interaction between the two monomers.

Once the CG model is validated against available experimental data and atomistic simulations, we discuss the effect of the monoclonal antibody Trastuzumab on the receptor dimerization at a molecular level. The simulation of the full receptor allows us to suggest an action mechanism for the Trastuzumab Fab while interacting with the ErbB2 dimer as follows. The binding of the Trastuzumab Fab to its native epitope at subdomain IV hinders the interaction of both ECDs through the subdomain IV

C-terminal fragment. This defective interaction causes in turn a small disruption of the transmembrane dimerization which is slightly displaced towards the C-terminal fragment. The JX segments in the intracellular domain should be affected by this displacement so that an antiparallel arrangement cannot be observed in our simulations. This lack of an antiparallel disposition might be associated to an inactive conformation of the TKD domain. The proposed mechanism is in line with the recent biological observations regarding the effective antibody deactivation on the proliferation signaling cascade initiated by the ErbB2 dimer [55].

Conclusions

We report, for the first time, molecular dynamics simulations of full models of ErbB2 monomer and dimer systems embedded in a lipid bilayer and complexed with the Trastuzumab-Fab monoclonal antibody.

The system has been simulated within the CG approach using the Martini force field. This force field is a well established model for molecular dynamics simulations of

systems containing proteins and lipids. The results presented in this paper support this assertion in view of the satisfactory comparison with experimental data and atomistic simulations.

Starting from the models proposed by Bagossi, we have carried out several μ s CG molecular dynamics simulations on systems containing either the full Erbb2 monomer or dimer with or without the monoclonal antibody Fab and embedded in a lipid bilayer.

The model proposed in this work seems to fulfill a number of experimental and computational observations about the full ErbB2 structure and its interaction with the lipid bilayer. Some details observed in atomistic simulations of the different ErbB domains are reproduced in the CG models. The most relevant observations are summarized below.

In the monomer case an interaction between the antibody constant domain and the dimerization arm can be observed in addition to the native interaction with the epitope in subdomain IV. This was also observed in atomistic simulations of the ECD.

The ErbB2 receptor extracellular domain tends to lay down on the lipid bilayer surface in agreement with recent FRET analysis and detailed atomistic simulations of homolog systems. The intracellular domain also presents a noticeable interaction with the bilayer surface. In particular, the JX fragment has been found to partially penetrate the membrane bilayer, in agreement with NMR measurements made with this fragment in a micelle environment.

The inclusion of the Trastuzumab Fab monoclonal antibody has a pronounced effect on the structural disposition of the ectodomain, due to the hindrance exerted on those amino acids mainly responsible for the interaction at subdomain IV C-terminal interaction. The antibody containing system shows a displacement towards the C-terminal segment of the transmembrane domain contacts in the dimer and a complete lost of the JX antiparallel arrangement characteristic of the active state that is also observed in the pure homodimer case. This action mechanism may explain the lost of signaling ability impaired by Trastuzumab to ErbB2 homodimers experimentally found.

Despite the misarrangement of the JX segments observed in the antibody case, the TKD dimer architecture is similar in both systems probably due to the tighter interaction in the initial Bagossi's model. The PCA analysis of the different trajectories reveals a rupture of the symmetric structure driving to a more asymmetric ensemble compatible with an active version of the TKD dimer.

Acknowledgments This study received financial support from the CICYT (projects MAT2009-12364 and MAT2012-36341). J.R. thanks to MINECO (Ministerio de Economía y Competitividad) the financial support through the *Ramón y Cajal* program, contract RYC-2011-09585. The authors thank the staff of the SGAI-CSIC

(Secretaría General Adjunta de Informática) for technical support and computer time for the simulations. We are also grateful to Prof. Bagossi for sharing his atomistic model in PDB format.

References

- Patel R, Leung HY (2012) Curr Pharm Des 18(19):2672
- Baselga J, Swain SM (2009) Nat Rev Cancer 9(7):463
- Slamon DJ, Clark GM, Wong SG, Levin WJ, Ullrich A, McGuire WL (1987) Science 235(4785):177
- Baselga J, Tripathy D, Mendelsohn J, Baughman S, Benz CC, Dantis L, Sklarin NT, Seidman AD, Hudis CA, Moore J, Rosen PP, Twaddell T, Henderson IC, Norton L (1996) J Clin Oncol 14(3):737
- Carter P, Presta L, Gorman CM, Ridgway JBB, Henner D, Wong WLT, Rowland AM, Kotts C, Carver ME, Shepard HM (1992) Proc Natl Acad Sci USA 89(10):4285
- Vogel CL, Cobleigh MA, Tripathy D, Gutheil JC, Harris LN, Fehrenbacher L, Slamon DJ, Murphy M, Novotny WF, Burchmore M, Shak S, Stewart SJ, Press M (2002) J Clin Oncol 20(3):719
- Nahta R (2012) Curr Med Chem 19(7):1065
- Nahta R, Esteva FJ (2006) Cancer Lett 232(2):123
- Nahta R, Esteva FJ (2007) Oncogene 26(25):3637
- Cho HS, Mason K, Ramyar KX, Stanley AM, Gabelli SB, Denney DW, Leahy DJ (2003) Nature 421(6924):756
- Franco-Gonzalez JF, Cruz VL, Ramos J, Martinez-Salazar J (2013) J Mol Model 19(3):1227
- Fuentes G, Scaltriti M, Baselga J, Verma CS (2011) Breast Cancer Res 13:R54
- Cho HS, Leahy DJ (2002) Science 297(5585):1330
- Du Y, Yang H, Xu Y, Cang X, Luo C, Mao Y, Wang Y, Qin G, Luo X, Jiang H (2012) J Am Chem Soc 134(15):6720
- Leahy DJ (2004) Cell Surf Recept 68:1
- Liu P, Bouyain S, Eigenbrot C, Leahy DJ (2012) Protein Sci 21(1):152
- Liu P, Cleveland TE, Bouyain S, Byrne PO, Longo PA, Leahy DJ (2012) Proc Natl Acad Sci USA 109(27):10861
- Beevers AJ, Kukol A (2006) J Mol Biol 361(5):945
- Bocharov EV, Mineev KS, Goncharuk MV, Arseniev AS (2012) Biochim Biophys Acta Biomembr 1818(9):2158
- Bocharov EV, Mineev KS, Volynsky PE, Ermolyuk YS, Tkach EN, Sobol AG, Chupin VV, Kirpichnikov MP, Efremov RG, Arseniev AS (2008) J Biol Chem 283(11):6950
- Garnier N, Crouzy S, Genest M (2003) J Biomol Struct Dyn 21(2):179
- Garnier N, Genest D, Duneau JP, Genest M (1997) Biopolymers 42(2):157
- Garnier N, Genest D, Genest M (1996) Biophys Chem 58(3):225
- Mineev KS, Bocharov EV, Pustovalova YE, Bocharova OV, Chupin VV, Arseniev AS (2010) J Mol Biol 400(2):231
- Mineev KS, Bocharov EV, Volynsky PE, Goncharuk MV, Tkach EN, Ermolyuk YS, Schulga AA, Chupin VV, Maslennikov IV, Efremov RG, Arseniev AS (2011) Acta naturae 3(2):90
- Prakash A, Janosi L, Doxastakis M (2010) Biophys J 99(11):3657
- Soumana OS, Garnier N, Genest M (2007) Eur Biophys J 36(8):1071
- Soumana OS, Garnier N, Genest M (2008) Eur Biophys J 37(6):851
- Lu P-C, Zhou C-F, Chen J, Liu P-G, Wang K-R, Mao W-J, Li H-Q, Yang Y, Xiong J, Zhu H-L (2010) Bioorg Med Chem 18(1):314
- Mustafa M, Mirza A, Kannan N (2011) Proteins Struct Funct Bioinform 79(1):99

31. Papakyriakou A, Vourloumis D, Tzortzatou-Stathopoulou F, Karpusas M (2009) *Proteins Struct Funct Bioinform* 76(2):375
32. Qiu C, Tarrant MK, Choi SH, Sathyamurthy A, Bose R, Banjade S, Pal A, Bornmann WG, Lemmon MA, Cole PA, Leahy DJ (2008) *Structure* 16(3):460
33. Qiu K-M, Wang H-H, Wang L-M, Luo Y, Yang X-H, Wang X-M, Zhu H-L (2012) *Bioorg Med Chem* 20(6):2010
34. Shi F, Telesco SE, Liu Y, Radhakrishnan R, Lemmon MA (2010) *Proc Natl Acad Sci USA* 107(17):7692
35. Shin AJ, Telesco SE, Choi S-H, Lemmon MA, Radhakrishnan R (2011) *Biochem J* 436:241
36. Telesco SE, Radhakrishnan R (2009) *Biophys J* 96(6):2321
37. Telesco SE, Shih AJ, Jia F, Radhakrishnan R (2011) *Mol BioSyst* 7(6):2066
38. Yun C-H, Mengwasser KE, Toms AV, Woo MS, Greulich H, Wong K-K, Meyerson M, Eck MJ (2008) *Proc Natl Acad Sci USA* 105(6):2070
39. Zhang X, Gureasko J, Shen K, Cole PA, Kuriyan J (2006) *Cell* 125(6):1137
40. Zhang X, Pickin KA, Bose R, Jura N, Cole PA, Kuriyan J (2007) *Nature* 450(7170):741
41. Kastner J, Loeffler HH, Roberts SK, Martin-Fernandez ML, Winn MD (2009) *J Struct Biol* 167(2):117
42. Martin-Fernandez ML (2012) *Biochem Soc Trans* 40:184
43. Roberts SK, Tynan CJ, Winn M, Martin-Fernandez ML (2012) *Biochem Soc Trans* 40:189
44. Bagossi P, Horvath G, Vereb G, Szollosi J, Tozser J (2005) *Biophys J* 88(2):1354
45. Arkhipov A, Shan Y, Das R, Endres NF, Eastwood MP, Wemmer DE, Kuriyan J, Shaw DE (2013) *Cell* 152(3):557
46. Marrink SJ, Tielemans DP (2013) *Chem Soc Rev* 42(16):6801
47. Marrink SJ, Risselada HJ, Yefimov S, Tielemans DP, de Vries AH (2007) *J Phys Chem B* 111(27):7812
48. Monticelli L, Kandasamy SK, Periole X, Larson RG, Tielemans DP, Marrink SJ (2008) *J Chem Theor Comput* 4(5):819
49. Hall BA, Chetwynd AP, Sansom MSP (2011) *Biophys J* 100(8):1940
50. Khalfa A, Tarek M (2010) *J Phys Chem B* 114(8):2676
51. Marrink SJ, de Vries AH, Tielemans DP (2009) *Biochim Biophys Acta. Biomembr* 1788(1):149
52. Felipe Franco-Gonzalez J, Ramos J, Cruz VL, Martinez-Salazar J (2013) *J Mol Model* 19(2):931
53. Vicente-Alique E, Nunez-Ramirez R, Francisco Vega J, Hu P, Martinez-Salazar J (2011) *Eur Biophys J* 40(7):835
54. Burgess AW, Cho HS, Eigenbrot C, Ferguson KM, Garrett TPJ, Leahy DJ, Lemmon MA, Sliwkowski MX, Ward CW, Yokoyama S (2003) *Mol Cell* 12(3):541
55. Ghosh R, Narasanna A, Wang SE, Liu S, Chakrabarty A, Balko JM, Gonzalez-Angulo AM, Mills GB, Penuel E, Winslow J, Sperinde J, Dua R, Pidaparthi S, Mukherjee A, Leitzel K, Kostler WJ, Lipton A, Bates M, Arteaga CL (2011) *Cancer Res* 71(5):1871
56. Periole X, Cavalli M, Marrink S-J, Ceruso MA (2009) *J Chem Theor Comput* 5(9):2531
57. Hess B, Kutzner C, van der Spoel D, Lindahl E (2008) *J Chem Theor Comput* 4(3):435
58. Essmann U, Perera L, Berkowitz ML, Darden T, Lee H, Pedersen LG (1995) *J Chem Phys* 103(19):8577
59. Berendsen HJC, Postma JPM, Vangunsteren WF, Dinola A, Haak JR (1984) *J Chem Phys* 81(8):3684
60. Hess B, Bekker H, Berendsen HJC, Fraaije J (1997) *J Comput Chem* 18(12):1463
61. Marrink SJ, de Vries AH, Mark AE (2004) *J Phys Chem B* 108(2):750
62. Amadei A, Linszen ABM, Berendsen HJC (1993) *Proteins Struct Funct Genet* 17(4):412
63. Amadei A, Linszen ABM, de Groot BL, van Aalten DMF, Berendsen HJC (1996) *J Biomol Struct Dyn* 13(4):615
64. Siuda I, Thogersen L (2013) *J Mol Model* 19(11):4931
65. Webb SED, Roberts SK, Needham SR, Tynan CJ, Rolfe DJ, Winn MD, Clarke DT, Barraclough R, Martin-Fernandez ML (2008) *Biophys J* 94(3):803
66. Lu C, Mi L-Z, Grey MJ, Zhu J, Graef E, Yokoyama S, Springer TA (2010) *Mol Cell Biol* 30(22):5432
67. Endres NF, Das R, Smith AW, Arkhipov A, Kovacs E, Huang Y, Pelton JG, Shan Y, Shaw DE, Wemmer DE, Groves JT, Kuriyan J (2013) *Cell* 152(3):543
68. Jura N, Endres NF, Engel K, Deindl S, Das R, Lamers MH, Wemmer DE, Zhang X, Kuriyan J (2009) *Cell* 137(7):1293
69. Chooowongkamon K, Carlin CR, Sonnichsen FD (2005) *J Biol Chem* 280(25):24043